

Nitric oxide elicits functional MMP-13 protein-tyrosine nitration during wound repair

Tania R. Lizarbe,* Concepción García-Rama,* Carlos Tarín,* Marta Saura,[†] Enrique Calvo,* Juan Antonio López,* Carlos López-Otín,[‡] Alicia R. Folgueras,[‡] Santiago Lamas,[§] and Carlos Zaragoza*¹

*Centro Nacional de Investigaciones Cardiovasculares, Madrid, Spain; [†]Departamento de Fisiología, Facultad de Medicina, Universidad de Alcalá, Madrid, Spain; [‡]Departamento de Bioquímica, Instituto Universitario de Oncología, Universidad de Oviedo, Oviedo, Spain; and [§]Centro de Investigaciones Biológicas, Instituto “Reina Sofía” de Investigaciones Nefrológicas, Madrid, Spain

ABSTRACT Nitric oxide (NO) plays a critical role in wound healing, in part by promoting angiogenesis. However, the precise repair pathways affected by NO are not well defined. We now show that NO regulates matrix metalloproteinase-13 (MMP-13) release during wound repair. We find that normally MMP-13 is kept inside endothelial cells by an association with caveolin-1. However, nitration of MMP-13 on tyrosine residue Y338 causes it to dissociate from caveolin-1 and be released from endothelial cells. We next explored the functional significance of MMP-13 nitration *in vivo*. Skin injury increases nitration of MMP-13 in mice. Skin wounds in inducible nitric oxide synthase knockout mice release less MMP-13 and heal more slowly than skin wounds in wild-type mice. Conversely, skin wounds in caveolin-1 knockout mice have increased NO production, increased MMP-13 nitration, and accelerated wound healing. Collectively, our data reveal a new pathway through which NO modulates wound repair: nitration of MMP-13 promotes its release from endothelial cells, where it accelerates angiogenesis and wound healing.—Lizarbe, T. R., García-Ram, C., Tarín, C., Saura, M., Calvo, E., López, J. A., López-Otín, C., Folgueras, A. R., Lamas, S., Zaragoza, C. Nitric oxide elicits functional MMP-13 protein-tyrosine nitration during wound repair. *FASEB J.* 22, 000–000 (2008)

Key Words: metalloproteinases · collagenase-3 · inducible nitric oxide synthase · caveolin-1 · wound healing

WOUND HEALING IS AN ORCHESTRATED task carried out in response to varied stimuli by several cell types (1–3), triggered by the release of several cytokines, growth factors, and radicals such as reactive oxygen species (4) and nitric oxide (NO). Mice lacking endothelial NO synthase have shown defects in wound healing and angiogenesis (5). However, the molecular mechanisms through which these molecules induce healing are still under investigation.

A critical determinant of cell migration is the balance that exists between extracellular matrix deposition and degradation. Matrix metalloproteinases (MMPs) are

extracellular matrix degrading enzymes that play essential roles during tissue development, atherosclerosis, ovarian function, arthritis, osteoarthritis, cancer, angiogenesis, and wound healing, processes that all involve cell migration (6–11). The matrix metalloproteinase MMP-13 is expressed by several cell types, including the vascular endothelium (12). MMP-13 forms a complex at the cell surface with caveolin-1, the major protein component of caveolae (13).

The role of caveolin-1 in cell migration has been proposed (14). We have identified a region within the C-terminal domain as the MMP-13 sequence that binds to caveolin-1, and we provide *in vitro* and *in vivo* evidence that NO triggers MMP-13 release and cell motility through posttranslational nitration of a tyrosine residue adjacent to this region.

MATERIALS AND METHODS

Reagents

General cell culture supplies were from BD Biosciences (Madrid, Spain), calf serum was from BioWhittaker (Verviers, Belgium), and cell culture gelatin and antibiotics were from Sigma (St. Louis, MO, USA). Autoradiography film was from Kodak (Rochester, NY, USA); polyvinylidene difluoride protein transfer membranes were from Millipore (Iberica, Spain); and horseradish peroxidase-conjugated secondary antibodies, the enhanced chemiluminescence immunoblot detection system, and protein A/G-Sepharose were from GE HealthCare (Alcobendas, Spain). EDTA-free protease inhibitor cocktail tablets were from Roche (Madrid, Spain). Opti-mem and Lipofectamine were from Gibco-Life Technologies (Gaithersburg, MD, USA). Fluorsave coverslip mounting solution was from Calbiochem (CN Biosciences, Nottingham, UK). The NO donor DEA-NO was from Alexis (Alexis Biochemicals, San Diego, CA, USA). Primary antibodies were obtained as follows: rabbit anti-human MMP-13 from Calbiochem; goat-anti-human-MMP-13 from Santa Cruz Biotechnologies (Santa Cruz, CA, USA); anti-caveolin-1 from BD Trans-

¹ Correspondence: Fundación CNIC, Melchor Fernández Almagro 3, 28029 Madrid, Spain. E-mail: czaragoza@cnic.es
doi: 10.1096/fj.07-103804

duction Laboratories (BD Biosciences); anti-FLAG from Sigma; and mouse monoclonal anti-ICAM-2 and VWF from Transduction Laboratories (BD Biosciences). The protein-nitration inhibitor peptide RYEYA was synthesized by Sigma.

Animals

Inducible nitric oxide synthase (iNOS) null mice and caveolin-1 null mice were purchased from The Jackson Laboratory (Bar Harbor, ME, USA). MMP-13 null mice were kindly donated by S. Krane (Center for Immunology and Inflammatory Diseases, Massachusetts General Hospital and Harvard Medical School, Charlestown, MA, USA). The background of all mice was C57BL/6, and therefore, C57BL/6 wild-type mice were used for control purposes. No differences in size and weight were detected in these mice. All animals were housed in our animal facilities in isolated rooms.

Cells

Bovine aortic endothelial cells (BAECs) and murine aortic endothelial cells (MAECs) were grown on gelatin (13). MAECs were selected by fluorescence-activated cell sorter with anti-ICAM-2 antibody, and culture purity was verified by double confocal immunofluorescence staining for VWF and ICAM-2. The purity of MAECs used in experiments exceeded 99%.

Plasmids and cell transfection

Epitope-tagged constructs encoding full-length MMP-13, partial and mutant MMP-13 sequences, and caveolin-1 were expressed in endothelial cells and in bacteria as indicated. In particular, we expressed the following MMP-13 polypeptides: full-length MMP-13 (amino acids 1–471); MMP-13 lacking the signal peptide (amino acids 20–471); MMP-13 lacking the propeptide domain (amino acids 112–471); MMP-13 catalytic domain (amino acids 112–267); MMP-13 hemopexin domain (HP; amino acids 281–471); and MMP-13 HP domain deletion mutant (lacking amino acids 347–360).

GST-fusion proteins were expressed with pGEX-4T2 (GE HealthCare). Recombinant proteins were purified as described previously (13). For mammalian expression, cDNAs were cloned in p3XFLAG-myc-CMV-24 (Sigma). Targeted deletion of HP domain was performed with the Quick Change Site-Directed Mutagenesis Kit (Stratagene, La Jolla, CA, USA).

For exogenous protein expression, cells were transiently transfected using Lipofectamine 2000 Reagent with the appropriate mammalian plasmids as described previously (13). Expression was monitored by confocal immunofluorescence microscopy and immunoblotting with the corresponding antibodies.

Wound-healing assay

Cells were grown in 6-well plates, and a straight cut was made across the confluent monolayer with a scalpel. Endothelial cell movement into the denuded area was monitored over time by microscopy as described previously (13).

Mouse skin repair and immunohistofluorescence

Mice were anesthetized, and after the dorsal hair was shaved and the skin was cleaned with ethanol, full-thickness excisional skin wounds were performed on the dorsal middle line using an 8 mm biopsy punch (Accuderm, Ft. Lauderdale, FL, USA). The healing was monitored by taking photographs at the indicated time points, and the area unoccupied by skin was calculated for each time point, using the Image J software (U.S. National Institutes of Health, Bethesda, MD, USA). Results were presented as percentage of original wound area at time point 0.

Skin biopsies were obtained from the back wounds of C57BL/6 wild-type iNOS null mice, MMP-13 null mice, and caveolin-1 null mice. Samples were embedded in paraffin, and 4 μ m thick serial sections were subjected to eosin-hematoxylin staining or confocal immunofluorescence microscopy with anti-MMP-13 and anti-nitrotyrosine antibodies as described previously (13).

Immunoblotting

Cell lysis and immunoblotting were performed as described previously (13).

Immunoprecipitation

Cells were disrupted with RIPA buffer, and lysates were precleared with the appropriate control immunoglobulin G (IgG) together with protein A-Sepharose. Immunoprecipitation was performed as described previously (13).

Confocal microscopy

Proteins were detected by confocal microscopy in cultured cells and paraffin-embedded tissue sections as described previously (13).

Affinity binding assays

Synthetic biotinylated peptides corresponding to the caveolin scaffolding domain (CSD) and to the caveolin-1 binding domain of MMP-13 (see **Table 1**) were purchased from

TABLE 1. Peptide sequences

Peptide	Sequence
MMP-13 peptides ^a	
CSD-BD	AYEHPSHDLIFIFRGRKFWALNGYD
CSD-BD DEL	YEHPSHDLIWALNGY
CSD-BD scramble	AYEHPSHDLIRRGFFFKIKWALNGYD
Caveolin-1 peptide, CSD	FHGIWKASFTTFTVTKYWFYRLL
Protein-nitration inhibitor peptide	RYEYA

^a Sequences based on residues 337–361, which span the 8-amino acid putative caveolin-1 binding sequence in the HP domain (underlined).

Sigma. Peptides were immobilized on neutravidin-loaded columns (Ultralink Immobilized Neutravidin Protein Plus; Pierce, Rockford, IL, USA), and recombinant purified proteins or cell extracts were passed through them. Columns were washed 3 times with 0.05% Tween 20 in PBS, and proteins were then eluted with 0.05 N NaOH for detection by immunoblot.

Metalloproteinase activity

MMP-13 activity was measured as the degradation of a fluorescent substrate from Calbiochem (CN Biosciences) as described by the manufacturer. The substrate is highly efficient for MMP-13, with low efficiency for MMP-1 and MMP-8.

Characterization of nitration of peptide HP

One milligram of biotinylated HP peptide was treated with 100 nM of ONOO⁻ for 10 min at room temperature. Nitrated HP peptide was digested by addition of modified porcine trypsin (sequencing grade; Promega, Madison, WI, USA) at a final concentration of 0.1 mg. Insoluble digestion proceeded at 37°C for 30 min. The resulting tryptic peptides were online injected onto a C-18 reversed-phase nanocolumn (Discovery BIO Wide Pore; Supelco, Bellefonte, PA, USA) and analyzed in a continuous acetonitrile gradient. A flow rate of ~300 nl/min was used to elute peptides from the reversed-phase nanocolumn to an electrospray ion source coupled to an ion trap mass spectrometer (Esquire HCT; Bruker Daltonics, Bremen, Germany) for real-time ionization and fragmentation.

Statistical analysis

Unless otherwise specified, data are expressed as means ± SD, and experiments were performed at least 3 times in duplicate. Whenever comparisons were made with a common control, comparisons were made with ANOVA followed by Dunnett's modification of the *t* test. The level of statistical significance was defined as *P* < 0.05. Error bars represent mean ± SD.

RESULTS

NO-mediated wound healing in mice is dependent on protein tyrosine nitration

To investigate the underlying effect of NO in wound repair (15, 16), we found that in iNOS null mice, cutaneous wound healing was significantly delayed with respect to wild-type mice (Fig. 1A, C; WT *vs.* iNOS). By contrast, blockage of protein nitration in excisional wounds (17; Table 1), prompted a similar pattern of wound closure in both animals (Fig. 1B, C; WT-N-Tyr-I *vs.* iNOS-N-Tyr-I), pointing toward nitration as one mechanism elicited by NO during wound repair.

MMP-13 nitration is involved in NO-mediated wound healing

We found that MMP-13 activity was induced in skin samples from wild-type injured animals with respect to iNOS null mice. However, tyrosine nitration inhibition significantly reduced MMP-13 activity in both strains

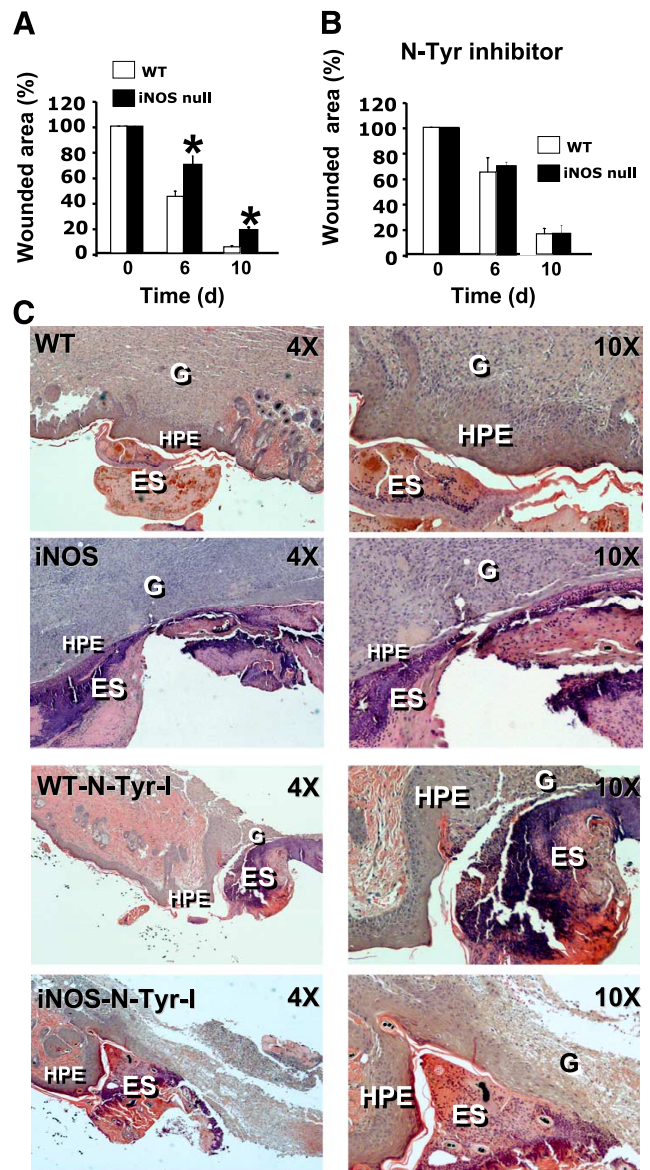


Figure 1. Lack of NO inhibits wound healing in mice. A) Wounds (8 mm) were made on the backs of wild-type (WT) and iNOS null mice, and area unoccupied by skin was monitored over time. Results are presented as percentage of initial wounded area (*n*=10 mice/time point; mean±SD; **P*<0.05 *vs.* time-matched WT). B) Same as in A and wounds were treated with N-tyrosine (N-Tyr) inhibitor peptide (100 μM) every day for 10 days (*n*=10 mice/time point). C) Eosin-hematoxylin staining of skin biopsies harvested 10 days after injury from WT mice (WT), iNOS null mice (iNOS), WT mice treated with the inhibitor peptide (WT-N-Tyr-I), and iNOS null mice treated with the inhibitor peptide (iNOS-N-Tyr-I). ES, Eschar; G, granulation tissue; HPE, hyperproliferative epithelium. View: ×4 (left panels); ×10 (right panels).

(Fig. 2A). In addition to MMP-13 activity, a correlation between protein nitration and wound healing was detected by confocal microscopy of skin biopsies from injured animals at day 6 posttreatment in which a substantial accumulation of nitrated MMP-13 in wild-type mice with respect to iNOS knockouts was detected, and this effect was reversed by protein nitration inhibition (Fig. 2B).

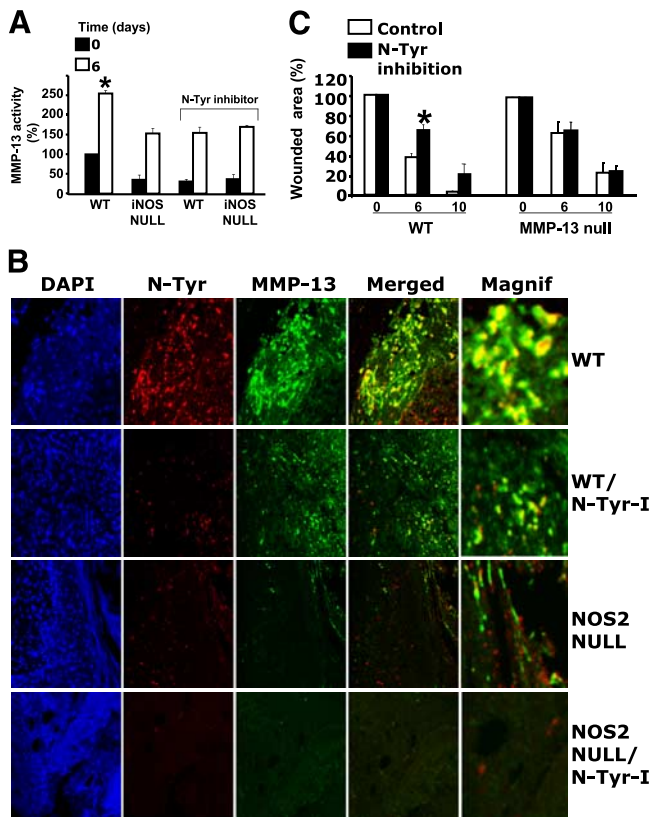


Figure 2. Nitration of MMP-13 is involved in NO-mediated wound healing. **A**) MMP-13 activity in skin collected from injured WT and iNOS null mice treated with N-Tyr inhibitory peptide as in Fig. 1B. Results are presented as absorbance units (mean \pm SD; * P < 0.05 WT 0 h vs. WT 6 h). **B**) Nitration of proteins (N-Tyr, green) and MMP-13 (red) detection by confocal microscopy of skin biopsies taken from WT and iNOS-deficient mice, treated or not every day with the N-Tyr inhibitory peptide and collected 6 days after injury. (n = 10 mice/time point). Cell nuclei were detected with DAPI. Merged panels show colocalization (yellow). **C**) Incisions were made on the backs of WT and MMP-13 null mice, treated or not with the N-Tyr inhibitory peptide, and the area unoccupied by skin was monitored over time. Results are presented as percentage of initial wounded area (n = 10 mice/time point; mean \pm SD; * P < 0.05 vs. N-Tyr inhibition).

The relevance of MMP-13 was also confirmed in MMP-13 null mice, detecting a significant delay of wound healing with respect to their wild-type counterparts. Interestingly, wound healing could not be further impaired by inhibition of protein tyrosine nitration in MMP-13 null mice, indicating the importance of MMP-13 nitration in wound repair (Fig. 2C).

Tyrosine nitration of MMP-13 mediates NO-induced MMP-13 secretion and endothelial cell migration during wound healing

We performed endothelial wound healing assays in BAECs in which we found that peroxynitrite (100 nmol/L) stimulated migration over control cells in a time-dependent manner, and this effect was prevented by the inhibition of nitration (Fig. 3A). In addition,

peroxynitrite also increased secreted MMP-13 activity in the conditioned media of injured cultures (Fig. 3B).

Tyrosine nitration of secreted MMP-13 was assayed by crossed coimmunoprecipitation of culture supernatants with anti-nitrotyrosine and anti-MMP-13 antibodies, detecting nitration of MMP-13 in the culture media of injured endothelial monolayers, with the signal strength increasing with the length of exposure to 100 nmol/L peroxynitrite (Fig. 3C).

Lack of caveolin-1 increases injury-dependent nitrogen stress and accelerates skin wound healing in mice

We and others found that MMP-13 binds to caveolin-1 (13) and that lack of caveolin-1 induces cell migration (18–20). To evaluate the relationship between MMP-13 and caveolin-1 in wound closure, we performed wound healing assays in caveolin-1 null mice. We found a significant acceleration of skin healing in caveolin-1 null mice, as compared with their wild-type counterparts (Fig. 4A, graph), detecting a significant increase of MMP-13 nitration (Fig. 4A, right panels) and MMP-13 activity (Fig. 4B, right graph) by day 6 after injury. In contrast, nitration inhibition induced wound closure delay (Fig. 4B, left graph), MMP-13 nitration reduction, and MMP-13 activity inhibition (Fig. 4B, bottom panels).

MMP-13 is bound to the cell membrane with caveolin-1 through the MMP HP-like domain

To explore the mechanism of NO-mediated MMP-13 nitration, we mapped the precise location at which MMP-13 binds to caveolin-1 in the plasma membrane before secretion. We generated FLAG-tagged polypeptides containing the following MMP-13 domains (Fig. 5A, top scheme): Full-length MMP-13, MMP-13 lacking the signal peptide (SP), MMP-13 lacking the propeptide domain (PP), the MMP-13 catalytic domain (CD), MMP-13 C-terminal domain (CTD), MMP-13 HP, and a variant of MMP-13 HP domain lacking amino acids 338 to 360 (HP*). We found that MMP-13 HP-like (FLAG-HP) was the single fragment of MMP-13 that shows colocalization with endogenous caveolin-1 (Fig. 5B, top panels), as detected by confocal microscopy and by crossed-coimmunoprecipitation.

For caveolin-1 ligands, a consensus binding motif has been proposed in which any three aromatic amino acid residues (\emptyset) are distributed as follows: $\emptyset X \emptyset XXX \emptyset$, (21). We identified a sequence with this structure (FIFRGRKF) in the MMP-13 HP domain at positions 347–354 (Fig. 5A, bottom scheme). Confocal microscopy, as well as coimmunoprecipitation assays showed that a version of the MMP-13 HP domain in which these 8 amino acids were deleted (FLAG-HP*) did not colocalize with caveolin-1 (Fig. 5B, bottom panels; Fig. 5C, right).

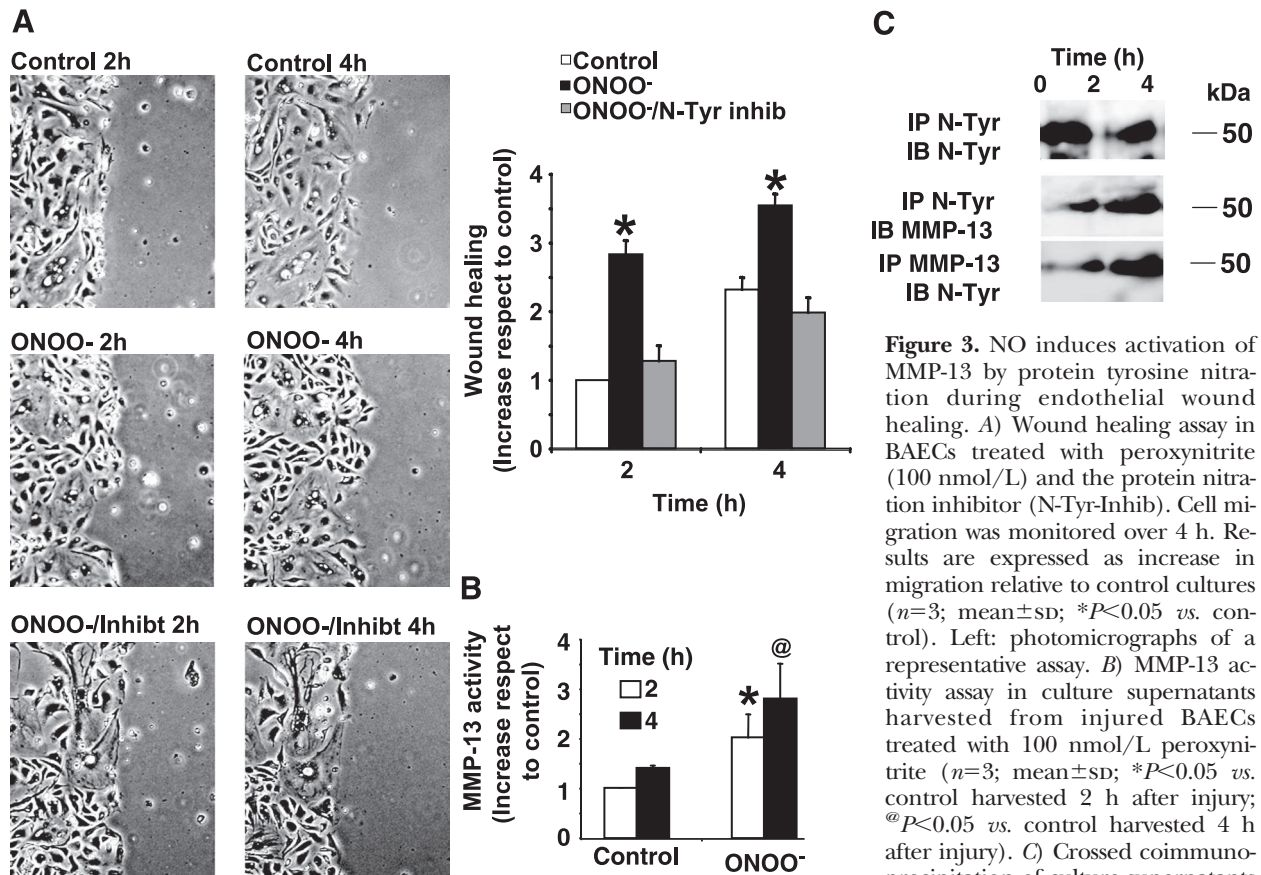


Figure 3. NO induces activation of MMP-13 by protein tyrosine nitration during endothelial wound healing. **A)** Wound healing assay in BAECs treated with peroxynitrite (100 nmol/L) and the protein nitration inhibitor (N-Tyr-Inhib). Cell migration was monitored over 4 h. Results are expressed as increase in migration relative to control cultures ($n=3$; mean \pm SD; $*P<0.05$ vs. control). Left: photomicrographs of a representative assay. **B)** MMP-13 activity assay in culture supernatants harvested from injured BAECs treated with 100 nmol/L peroxynitrite ($n=3$; mean \pm SD; $*P<0.05$ vs. control harvested 2 h after injury; $@P<0.05$ vs. control harvested 4 h after injury). **C)** Crossed coimmunoprecipitation of culture supernatants

from BAECs treated as in **B**. Culture supernatants were immunoprecipitated (IP) with anti-nitrotyrosine antibody (N-Tyr) and with anti-MMP-13 antibody, and proteins were detected by immunoblot (IB). As loading control, immunoprecipitated supernatants with anti-nitrotyrosine were also detected with anti-nitrotyrosine antibody ($n=3$).

2NO disrupts interaction between the MMP-13 HP domain and the scaffolding domain of caveolin-1

We exposed endothelial cells expressing FLAG-HP to the NO donor DEA-NO (10 or 100 nmol/L, liberating 15 nmol and 150 nmol of NO, respectively), finding inhibition of the capacity to interact with caveolin-1 at either DEA-NO concentration, as detected by crossed coimmunoprecipitation (Fig. 5D) and confocal microscopy (Fig. 5E).

To further dissect the contribution of NO, we carried out affinity-binding reactions with biotinylated peptides corresponding to wild-type and mutant sequences of the putative CSD-binding domain (CSD-BD) of MMP-13 (Table 1). Columns bearing the wild-type peptide (CSD-BD) retained caveolin-1 from BAEC lysates (Fig. 6A, lane 2), but peptides in which the consensus 8-amino acid CSD binding sequence was deleted (CSD-BD DEL) or scrambled (CSD-BD scramble) did not (Fig. 6A, lanes 3 and 4). When peptides were pretreated with 100 nmol/L DEA-NO, caveolin-1 was not retained by any of the columns (Fig. 6A, lanes 5–8). Similar results were obtained with MAEC lysates (Fig. 6B).

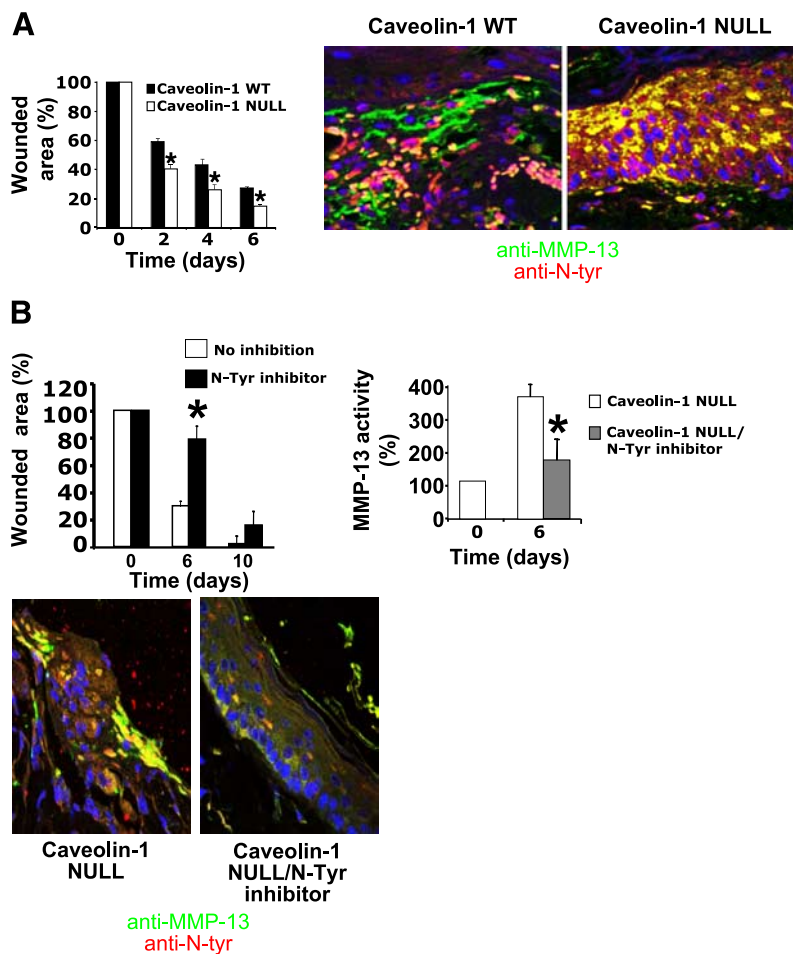
We next tested the ability of columns bearing a biotinylated caveolin-1 scaffolding domain (CSD) peptide, used to bind to other proteins, to bind purified

recombinant GST-fusion versions of MMP-13. Full-length MMP-13 (GST-MMP-13) and the MMP-13-HP domain (GST-HP) bound to the CSD, but no interaction was detected with the MMP-13 HP domain lacking the CSD-BD (GST-HP CSD-BD DEL) (Fig. 6C, lanes 1 and 3 vs. lane 5). Incubation of GST-fusion proteins with 100 nmol/L DEA-NO, significantly reduced binding of GST-MMP-13 (Fig. 6C, lane 1 vs. lane 2) and completely blocked binding of GST-HP (Fig. 6C, lane 3 vs. lane 4). These results demonstrate that MMP-13 and caveolin-1 interact through the CSD-BD and the CSD, respectively, and that NO disrupts the complex.

MMP-13 tyrosine 338 is required for binding to caveolin-1 and is a target of NO-mediated protein tyrosine nitration

Interestingly, we found that flanking the CSD-BD domain were two tyrosine residues present at positions 338 and 360 of the MMP-13, respectively (Fig. 7A). Endothelial cells were transfected with FLAG-tagged wild-type MMP-13 (MMP-13 WT) or with one of two FLAG-tagged MMP-13 constructs containing a point mutation at one of the tyrosine residues: MMP-13-Y338F and MMP-13-Y360F (Fig. 7B), detecting that exogenously MMP-13 WT and MMP-13-Y360F were bound caveolin-1 (Fig. 7B, left and right panels); how-

Figure 4. Tyrosine nitration inhibition in caveolin-1 null mice delays wound healing at the levels of WT animals. **A)** Left: incisions were made on the backs of WT and caveolin-1 null mice, and area unoccupied by skin was monitored over time. Results are presented as percentage of initial wounded area ($n=10$ mice/time point; mean \pm sd; $*P<0.05$ vs. time-matched WT). Right: representative micrograph showing detection of MMP-13 (green) and protein nitration (red) by confocal microscopy of skin biopsies taken 6 days after injury ($n=10$). Colocalization of two signals is detected in yellow. Cell nuclei were stained with DAPI. **B)** Left: incisions were made on the backs of WT and caveolin-1 null mice in the presence or absence of tyrosine nitration inhibition ($n=10$ mice/time point; mean \pm sd; $*P<0.05$ vs. N-Tyr inhibitor). Right, top graph: MMP-13 activity in skin collected from caveolin-1 null mice treated with N-Tyr inhibitory peptide (100 μ mol/L). Results are presented as percentage of MMP-13 activity detected in untreated mice at time point 0 (mean \pm sd; $*P<0.05$). Bottom: representative micrograph showing detection of MMP-13 (green) and protein nitration (red) by confocal microscopy of skin biopsies taken 6 days after injury ($n=10$). Colocalization of two signals is detected in yellow. Cell nuclei were stained with DAPI.



ever, MMP-13-Y338F did not (Fig. 7B, middle panels), indicating that tyrosine 338 is required for binding of MMP-13 to caveolin-1.

We therefore tried to characterize protein nitration of tyrosine 338 of MMP-13. By incubation of the MMP-13 CSD-BD-peptide with peroxynitrite (100 nmol/L) and further mass spectrometric analysis, we detected a singly nitrated peptide corresponding to tyrosine 338 (Fig. 7C, D), and no signal was detected corresponding to modification of the second tyrosine residue. These results identify tyrosine 338 as the target for NO-mediated nitration of MMP-13 and support a role for this event in NO-mediated disruption of the binding of MMP-13 to caveolin-1.

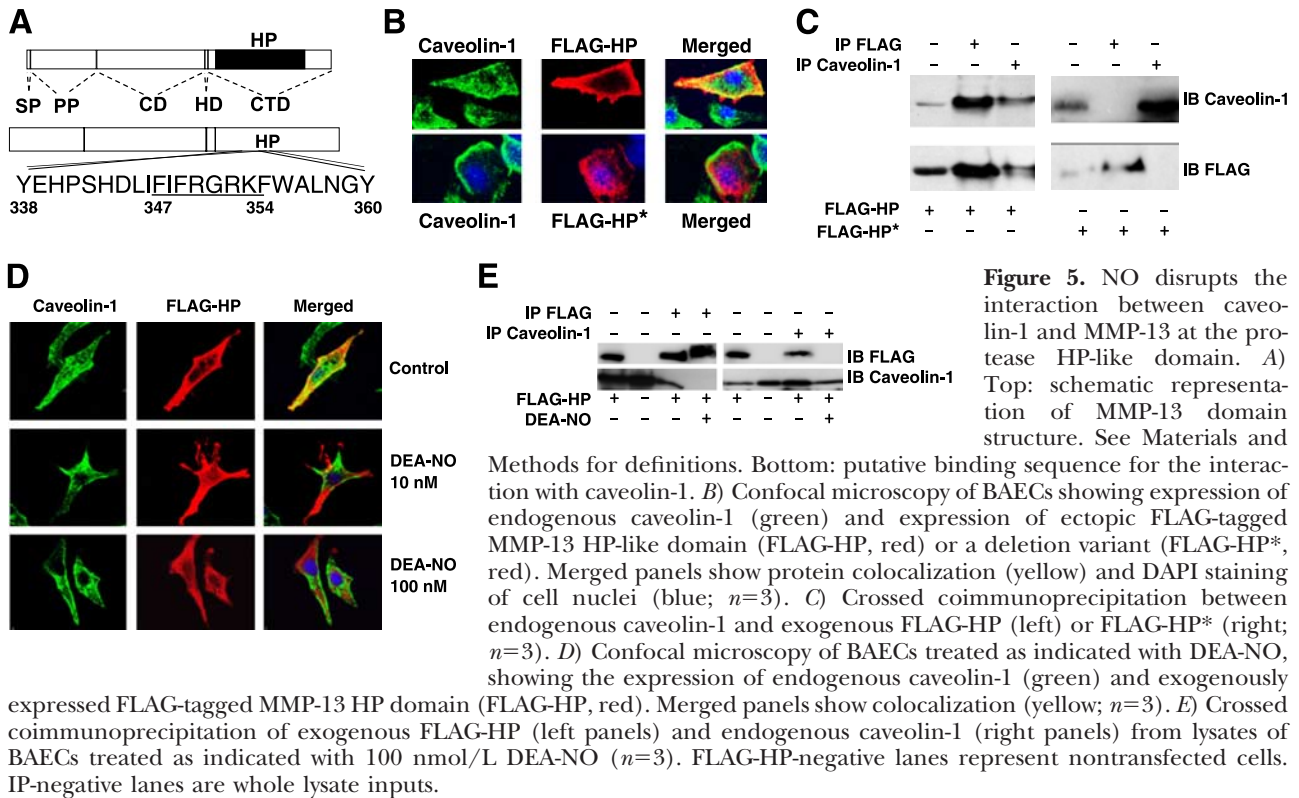
DISCUSSION

Our data provide evidence that MMP-13 nitration at residue Tyr-338 is a mechanism through which NO releases and activates MMP-13 during endothelial migration and wound repair. In iNOS null mice, protein nitration was significantly reduced, as well as MMP-13 activity and repair. Wound healing was similarly impaired in MMP-13 null mice, and both knockouts mimicked the effect of the tyrosine nitration inhibitor in wild-type animals. Most significantly, wound healing

in these deficient mice could not be further impaired by inhibiting protein tyrosine nitration. These experiments thus show that MMP-13 is required for tyrosine nitration-dependent wound healing, providing evidence for an association between tyrosine nitration and MMP-13 activation.

Although earlier studies (13, 14, 22) identified caveolin-1 interaction with distinct MMPs, this is the first identification of an MMP domain responsible for the interaction with caveolin-1 (CSD-BD), which includes the 8-amino acid motif FIFRGRKF (21). The CSD-BD is flanked by two tyrosine residues. Substitution of tyrosine 338 with phenylalanine abolished the association between MMP-13 and caveolin-1, demonstrating that this residue is required for the interaction of these proteins.

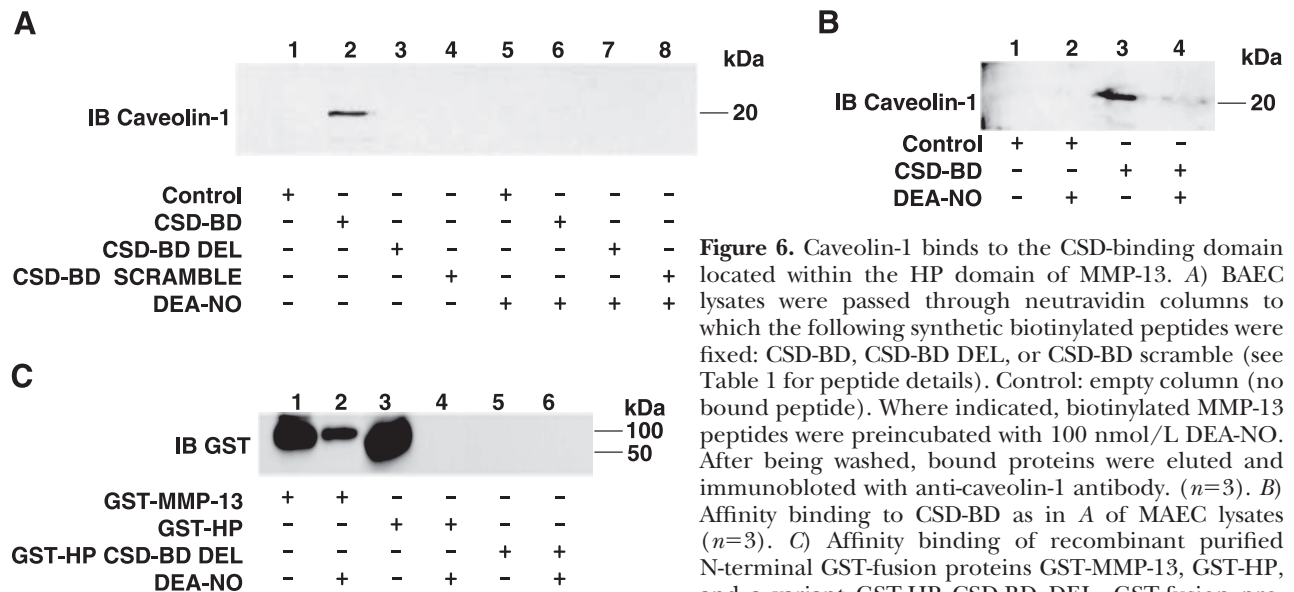
Caveolin-1 functions as a membrane dock for many proteins involved in intracellular signaling and, in general, impedes the function of the proteins it binds to (23, 24). In addition to MMP-13, caveolin-1 colocalizes with and impedes the function of the extracellular matrix degrading enzymes MMP-2 and MMP-9 (25), with the exception of MT1-MMP, which requires caveolin-1 binding for its activity (26), although MT1-MMP is membrane bound and is not released from cells to exert its activity. Release and activity of MMPs 2 and 9 are increased by gene knockout of caveolin-1 and



impeded by its reexpression, whereas CSD peptideinhibits cell migration associated with these proteases (14), supporting our finding as a general mechanism shared by other MMPs. In addition, in caveolin-1-deficient mice wound repair was accelerated, and it was associated with increased nitrotyrosine staining and increased MMP-13 activity at the wound site. The increased nitration may arise from increased endothelial NO synthase activity, since this is normally re-

strained by binding to caveolin-1 and is increased in caveolin-1-deficient animals (27).

Our results suggests that nitration might be required for dissociation from caveolin-1 and proteolytic activation of unbound MMP-13. However, we cannot exclude involvement of NO-induced S-nitrosylation, as described for MMP-9 activation in the CNS (28). Another possibility is that MMP-13 also interacts with a yet undefined partner, and dissociation also requires NO.



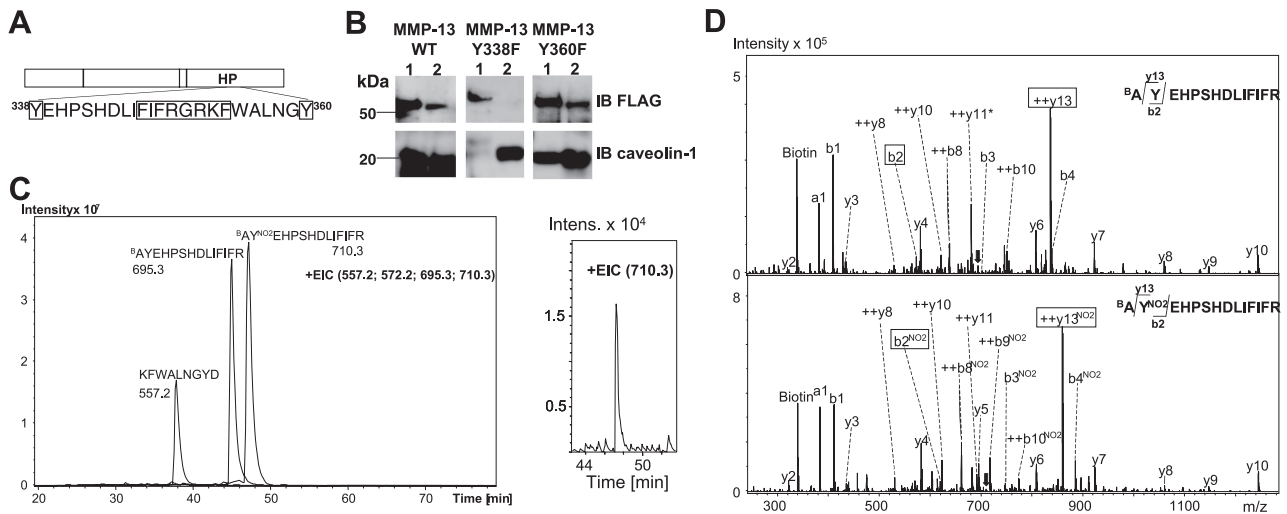


Figure 7. NO induces nitration of tyrosine 338 of MMP-13, required for the binding to caveolin-1. *A*) Schematic representation of MMP-13 caveolin-1 binding domain. *B*) Crossed coimmunoprecipitation of lysates from BAECs expressing FLAG-tagged WT MMP-13 (MMP-13-WT) or point-mutated versions in which tyrosines at positions 338 or 360 were substituted by proline (MMP-13-Y338F and MMP-13-Y360F). Lane 1: immunoprecipitation with anti-FLAG; lane 2: immunoprecipitation with anti-caveolin-1 ($n=3$). *C*) Left: extracted ion chromatogram (EIC) of digested CSD-BD peptides. N-terminally biotinylated (B) CSD-BD peptide was treated with 100 $\mu\text{mol/L}$ ONOO^- , digested with trypsin, and analyzed by electrospray ionization-ion trap mass spectrometry as described in Materials and Methods. Chart shows EIC for the ions at m/z 557.2 Da (doubly-charged peptide KFWALNGYD) and 695.3 Da (triple charged peptide $^{\text{B}}\text{AYEHPSHDLIFIFR}$) and their corresponding tyrosine-nitrated peptides (m/z 572.2 and 710.3 Da). These peptides correspond to C- and N-terminal portions of the CSD-BD, respectively. The two unmodified peptides were detected, but the only nitrated ion detected was m/z 710.3 Da, containing the nitrated Tyr-338. Right inset: EIC chart for the ion at m/z 710.3 Da, as a result of treatment with 100 nmol/L ONOO^- ; no signal was detected for peptide containing second nitrated tyrosine at any ONOO^- concentration. *D*) Protein sequencing and characterization of digested CSD-BD peptides. MS/MS spectra from ions at m/z 695.3 (top panel) and 710.3 Da (bottom panel), corresponding to unmodified and tyrosine-nitrated $^{\text{B}}\text{AYEHPSHDLIFIFR}$. Diagram shows fragment ions corresponding to main fragmentation series (*, water loss; ++, doubly charged fragments). Numbered boxes indicate nitration revealed by both b and y series.

Previous studies (21) show that at least four of the five residues critical for binding to the caveolin-1 CSD are aromatic (CSD residues F89, F92, W98, and F99), suggesting that the interactions are mainly hydrophobic. Modeling of the three-dimensional structure of the human MMP-13 HP domain (29) predicts that residues F347, F349, and F354, together with Y338, form a hydrophobic pocket oriented toward the outer surface of the HP domain. The relative positioning of these aromatic side chains suggests that CSD F89 might interact with MMP-13 Y338 through hydrophobic and van der Waals forces. Nitration of MMP-13 Y338 would then abolish this interaction, probably by reducing the hydrophobicity and thereby disrupting the MMP-13 HP hydrophobic pocket, and this may be a general mechanism for dissociation from caveolin-1.

Tyrosine nitration modulates the activity of several proteins and is associated with many pathological situations, including Alzheimer's, Parkinson's (30), and cardiovascular diseases (31). Protein tyrosine nitration of MMP-13 by physiologically relevant concentrations of peroxynitrite at Tyr 338 provides a mechanistic explanation of how NO disrupts the MMP-13/caveolin-1 complex and initiates cell migration (13, 32, 33).

Activation of cell migration through NO-induced protein nitration has implications for the understanding of endothelial activation in a range of physiological and pathological situations, including angiogenesis,

atherosclerosis and cancer, and the ability to identify such early activation events may provide markers of the initial stages of endothelial dysfunction. [F]

This study was supported by the following institutions and agencies: Ministerio de Educación y Ciencia, Programa Ramón y Cajal (to C.Z. and M.S.); Plan Nacional de I+D+I (SAF 2005-06025 to C.Z. and SAF 2006-02410 to S.L.); the European Union (FEDER 2FD97-1432, to S.L.); the Spanish Society of Nephrology (grant-in-aid 2001, to C.Z. and S.L.); and the Ministerio de Sanidad y Consumo (Red temática de investigación cooperativa RECAVA C03/01, to C.Z. and S.L.). We thank Dr. S. Bartlett for valuable and significant assistance with the manuscript.

REFERENCES

1. Navarro, A., Anand-Apte, B., and Parat, M. O. (2004) A role for caveolae in cell migration. *FASEB J.* **18**, 1801-1811
2. Gerhardt, H., and Betsholtz, C. (2005) How do endothelial cells orientate? *EXS* 3-15
3. Nairi, E., Lee, E., Testa, J., Quigley, J., Colflesh, D., Keese, C. R., Giaever, I., and Goligorsky, M. S. (1998) Podokinesis in endothelial cell migration: role of nitric oxide. *Am. J. Physiol.* **274**, C236-C244
4. Yung, L. M., Leung, F. P., Yao, X., Chen, Z. Y., and Huang, Y. (2006) Reactive oxygen species in vascular wall. *Cardiovasc. Hematol. Disord. Drug Targets* **6**, 1-19
5. Lee, P. C., Salyapongse, A. N., Bragdon, G. A., Shears, L. L., 2nd, Watkins, S. C., Edington, H. D., and Billiar, T. R. (1999)

- Impaired wound healing and angiogenesis in eNOS-deficient mice. *Am. J. Physiol.* **277**, H1600–H1608
6. Newby, A. C. (2006) Matrix metalloproteinases regulate migration, proliferation, and death of vascular smooth muscle cells by degrading matrix and non-matrix substrates. *Cardiovasc. Res.* **69**, 614–624
 7. Lynch, C. C., and Matrisian, L. M. (2002) Matrix metalloproteinases in tumor-host cell communication. *Differentiation* **70**, 561–573
 8. Ravanti, L., and Kahari, V. M. (2000) Matrix metalloproteinases in wound repair (review). *Int. J. Mol. Med.* **6**, 391–407
 9. Kuzuya, M., and Iguchi, A. (2003) Role of matrix metalloproteinases in vascular remodeling. *J. Atheroscler. Thromb.* **10**, 275–282
 10. Inada, M., Wang, Y., Byrne, M. H., Rahman, M. U., Miyaura, C., Lopez-Otin, C., and Krane, S. M. (2004) Critical roles for collagenase-3 (Mmp13) in development of growth plate cartilage and in endochondral ossification. *Proc. Natl. Acad. Sci. U. S. A.* **101**, 17192–17197
 11. Zucker, S., Cao, J., and Chen, W. T. (2000) Critical appraisal of the use of matrix metalloproteinase inhibitors in cancer treatment. *Oncogene* **19**, 6642–6650
 12. Zaragoza, C., Balbin, M., Lopez-Otin, C., and Lamas, S. (2002) Nitric oxide regulates matrix metalloproteinase-13 expression and activity in endothelium. *Kidney Int.* **61**, 804–808
 13. Lopez-Rivera, E., Lizarbe, T. R., Martinez-Moreno, M., Lopez-Novoa, J. M., Rodriguez-Barbero, A., Rodrigo, J., Fernandez, A. P., Alvarez-Barrientos, A., Lamas, S., and Zaragoza, C. (2005) Matrix metalloproteinase 13 mediates nitric oxide activation of endothelial cell migration. *Proc. Natl. Acad. Sci. U. S. A.* **102**, 3685–3690
 14. Williams, T. M., Medina, F., Badano, I., Hazan, R. B., Hutchinson, J., Muller, W. J., Chopra, N. G., Scherer, P. E., Pestell, R. G., and Lisanti, M. P. (2004) Caveolin-1 gene disruption promotes mammary tumorigenesis and dramatically enhances lung metastasis in vivo. Role of Cav-1 in cell invasiveness and matrix metalloproteinase (MMP-2/9) secretion. *J. Biol. Chem.* **279**, 51630–51646
 15. Weller, R. (2003) Nitric oxide: a key mediator in cutaneous physiology. *Clin. Exp. Dermatol.* **28**, 511–514
 16. Yamasaki, K., Edington, H. D., McClosky, C., Tzeng, E., Lizonova, A., Kovesdi, I., Steed, D. L., and Billiar, T. R. (1998) Reversal of impaired wound repair in iNOS-deficient mice by topical adenoviral-mediated iNOS gene transfer. *J. Clin. Invest.* **101**, 967–971
 17. Ye, Y., Quijano, C., Robinson, K. M., Ricart, K. C., Strayer, A. L., Sahawneh, M. A., Shacka, J. J., Kirk, M., Barnes, S., Accavitti-Loper, M. A., Radi, R., Beckman, J. S., and Estevez, A. G. (2007) Prevention of peroxynitrite-induced apoptosis of motor neurons and PC12 cells by tyrosine-containing peptides. *J. Biol. Chem.* **282**, 6324–6337
 18. Hassan, G. S., Williams, T. M., Frank, P. G., and Lisanti, M. P. (2006) Caveolin-1-deficient aortic smooth muscle cells show cell autonomous abnormalities in proliferation, migration, and endothelin-based signal transduction. *Am. J. Physiol. Heart Circ. Physiol.* **290**, H2393–2401
 19. Kim, H. P., Wang, X., Nakao, A., Kim, S. I., Murase, N., Choi, M. E., Ryter, S. W., and Choi, A. M. (2005) Caveolin-1 expression by means of p38beta mitogen-activated protein kinase mediates the antiproliferative effect of carbon monoxide. *Proc. Natl. Acad. Sci. U. S. A.* **102**, 11319–11324
 20. Zhang, W., Razani, B., Altschuler, Y., Bouzahzah, B., Mostov, K. E., Pestell, R. G., and Lisanti, M. P. (2000) Caveolin-1 inhibits epidermal growth factor-stimulated lamellipod extension and cell migration in metastatic mammary adenocarcinoma cells (MTLn3). Transformation suppressor effects of adenovirus-mediated gene delivery of caveolin-1. *J. Biol. Chem.* **275**, 20717–20725
 21. Couet, J., Li, S., Okamoto, T., Ikezu, T., and Lisanti, M. P. (1997) Identification of peptide and protein ligands for the caveolin-scaffolding domain. Implications for the interaction of caveolin with caveolae-associated proteins. *J. Biol. Chem.* **272**, 6525–6533
 22. Labrecque, L., Nyalendo, C., Langlois, S., Durocher, Y., Roghi, C., Murphy, G., Gingras, D., and Beliveau, R. (2004) Src-mediated tyrosine phosphorylation of caveolin-1 induces its association with membrane type 1 matrix metalloproteinase. *J. Biol. Chem.* **279**, 52132–52140
 23. Stan, R. V. (2005) Structure of caveolae. *Biochim. Biophys. Acta* **1746**, 334–348
 24. Pike, L. J. (2005) Growth factor receptors, lipid rafts and caveolae: an evolving story. *Biochim. Biophys. Acta* **1746**, 260–273
 25. Puyraimond, A., Fridman, R., Lemesle, M., Arbeille, B., and Menashi, S. (2001) MMP-2 colocalizes with caveolae on the surface of endothelial cells. *Exp. Cell. Res.* **262**, 28–36
 26. Galvez, B. G., Matias-Roman, S., Yanez-Mo, M., Vicente-Manzanares, M., Sanchez-Madrid, F., and Arroyo, A. G. (2004) Caveolae are a novel pathway for membrane-type 1 matrix metalloproteinase traffic in human endothelial cells. *Mol. Biol. Cell* **15**, 678–687
 27. Razani, B., Engelman, J. A., Wang, X. B., Schubert, W., Zhang, X. L., Marks, C. B., Macaluso, F., Russell, R. G., Li, M., Pestell, R. G., Di Vizio, D., Hou, H., Jr., Kneitz, B., Lagaud, G., Christ, G. J., Edelmann, W., and Lisanti, M. P. (2001) Caveolin-1 null mice are viable but show evidence of hyperproliferative and vascular abnormalities. *J. Biol. Chem.* **276**, 38121–38138
 28. Gu, Z., Kaul, M., Yan, B., Kridel, S. J., Cui, J., Strongin, A., Smith, J. W., Liddington, R. C., and Lipton, S. A. (2002) S-nitrosylation of matrix metalloproteinases: signaling pathway to neuronal cell death. *Science* **297**, 1186–1190
 29. Gomis-Ruth, F. X., Gohlke, U., Betz, M., Knauper, V., Murphy, G., Lopez-Otin, C., and Bode, W. (1996) The helping hand of collagenase-3 (MMP-13): 2.7 Å crystal structure of its C-terminal haemopexin-like domain. *J. Mol. Biol.* **264**, 556–566
 30. Ebadi, M., Brown-Borg, H., El Refaey, H., Singh, B. B., Garrett, S., Shavali, S., and Sharma, S. K. (2005) Metallothionein-mediated neuroprotection in genetically engineered mouse models of Parkinson's disease. *Brain Res. Mol. Brain Res.* **134**, 67–75
 31. Turko, I. V., and Murad, F. (2002) Protein nitration in cardiovascular diseases. *Pharmacol. Rev.* **54**, 619–634
 32. Beare, A. H., O'Kane, S., Krane, S. M., and Ferguson, M. W. (2003) Severely impaired wound healing in the collagenase-resistant mouse. *J. Invest. Dermatol.* **120**, 153–163
 33. Hartenstein, B., Dittrich, B. T., Stickens, D., Heyer, B., Vu, T. H., Teurich, S., Schorpp-Kistner, M., Werb, Z., and Angel, P. (2006) Epidermal development and wound healing in matrix metalloproteinase 13-deficient mice. *J. Invest. Dermatol.* **126**, 486–496

Received for publication January 25, 2008.

Accepted for publication April 24, 2008.